Biochimica et Biophysica Acta 1850 (2015) 673–680

Contents lists available at ScienceDirect

Biochimica et Biophysica Acta

journal homepage: www.elsevier.com/locate/bbagen

Molecular recognition in naphthoquinone derivatives — G-quadruplex complexes by NMR

Benedetta Riva [a], Ruben Ferreira [b,1], Loana Musso [c], Roberto Artali [d], Leonardo Scaglioni [c], Stefania Mazzini [c,*]

[a] Department of Biotechnology and Biosciences, University of Milano-Bicocca, Piazza della scienza 3, 20126 Milan, Italy
[b] Department of Chemical and Biological Engineering, Chalmers University of Technology SE-412 96 Göteborg, Sweden
[c] Department of Food, Environmental and Nutritional Sciences, Division of Chemistry and Molecular Biology, University of Milan, Via Celoria 2, 20133 Milan, Italy
[d] Scientia Advice, Desio, Italy

ARTICLE INFO

Article history:
Received 4 August 2014
Received in revised form 4 November 2014
Accepted 2 December 2014
Available online 11 December 2014

Keywords:
G-quadruplex
NMR studies
DNA-binding drugs
Isoxazolo naphthoquinone
Molecular modeling

ABSTRACT

Background: G-quadruplexes have become important drug-design targets for the treatment of various human disorders such as cancer, diabetes and cardiovascular diseases. Recently, G-quadruplex structures have been visualized in the DNA of human cells and appeared to be dynamically sensitive to the cell cycle and stabilized by small molecule ligands. A small library of isoxazolo naphthoquinones (**1a**–**h**), which exhibited a strong antiproliferative activity on different cancer cell lines, was studied as potential ligands of G-quadruplex DNA.
Methods: The DNA binding properties of a series of the selected compounds have been analyzed by fluorescence assays. NMR/modeling studies were performed to describe the complexes between G-quadruplex DNA sequences and two selected compounds **1a** and **1b**.
Results: **1a** and **1b** in the presence of G-quadruplexes, $d(T_2AG_3T)_4$, $d(TAG_3T_2A)_4$ and $d(T_2G_3T_2)_4$, showed good ability of intercalation and the formation of complexes with 2:1 stoichiometry. **1a** showed an important interaction with the sequence Pu22 belonging to the promoter of oncogenes *c-myc*.
Conclusions: The ligands directly interact with the external G-tetrads of the G-quadruplexes, without alterations in the structure of the G-quadruplex core. The role of the adenine moieties over the G-tetrads in the stabilization of the complexes was discussed.
General significance: The results obtained suggested that the strong antiproliferative activity of isoxazolo naphthoquinones is not due to the Hsp90 inhibition, but mainly to the interaction at the level of telomeres and/or at the level of gene promoter. These findings can be used as a basis for the rational drug design of new anticancer agents.

© 2014 Elsevier B.V. All rights reserved.

1. Introduction

The interest toward G-quadruplex DNA is mainly due to the presence of guanine-rich sequences, potentially able to form these structures, in crucial regions of human genome [1], such as telomeric ends [2], ribosomal DNA (rDNA) [3], RNA or gene promoter regions (*c-myc*, *bcl-2*, or *c-kit*) [4–6]. The aberrant overexpression of the proto-oncogene *c-myc* is associated with a large number of human tumors and its transcriptional regulation has been extensively studied [7–10]. There is a particular region of *c-myc* gene rich in purines that generally regulates 80–90% of its transcription and is able to form a G-quadruplex structure useful for silencing the transcription [11–13].

G-quadruplex structures have been recently visualized in the DNA of human cells [14], demonstrating that the formation of G-quadruplexes is dynamically sensitive to the cell cycle, and that endogenous G-quadruplex DNA structures can be stabilized by small molecule ligands. As a result, G-quadruplexes have become important drug targets for the treatment of various human disorders such as cancer [15,16], diabetes [17], and cardiovascular diseases [18]. The concept of targeting G-quadruplexes as a therapeutic strategy was first developed for telomeric DNA and telomerase inhibition [19]. Telomerases are present in 80–85% of human tumor cells while they are essentially absent in normal cells [20]. These observations have generated great interest in the potential of the telomeres and telomerase as anticancer target, the enzymatic activity of telomerase [21] being inhibited by the formation of stabilized G-quadruplex structures.

In the past two decades, hundreds of small molecules, with diverse chemical structures and physicochemical properties, have been designed to bind selectively and with high affinity to telomeric G-quadruplex [22,23]. Most of these molecules have been found to interact by π-stacking with the wide aromatic surface of the G-tetrads at the 5′ and/or 3′-edge of the G-quadruplex. However, the ligands can also be located into the grooves or interact with the loop bases [24,25].

* Corresponding author. Tel.: +39 02 50316813; fax: +39 02 50316801.
E-mail addresses: b.riva10@campus.unimib.it (B. Riva), rubenf@chalmers.se (R. Ferreira), stefania.mazzini@unimi.it (S. Mazzini).
[1] Tel.: +46 31 786 90 94; fax: +46 31 772 38 58.

http://dx.doi.org/10.1016/j.bbagen.2014.12.002
0304-4165/© 2014 Elsevier B.V. All rights reserved.

In a previous paper [26] we reported the synthesis of a small library of isoxazolo-fused naphthoquinones that showed a strong antiproliferative activity on different human tumor cell lines (not small-lung cancer NCI-H460, A431 squamous cell carcinoma, peritoneal mesothelioma STO). Despite these molecules were designed as potential inhibitors of the heat shock protein 90 (Hsp90) [27], they did not exhibit a strong interaction with this protein, and their molecular targets still remain unknown. The idea of investigating these molecules as G-quadruplex DNA ligands was inspired by the observation of the structures of some of them: compounds **1a**–**h** (Fig. 1) appear able to give both π-stacking interactions, through the aromatic system of naphthoquinone moiety, and electrostatic interactions, through the quaternary salt in the side-arm. Molecules with similar structures were previously studied as G-quadruplex stabilizing ligands, mainly addressed to inhibit the proto-oncogene *c-kit* [28–30]. In our work we studied compounds **1a**–**h** as potential stabilizers/ligands of different G-quadruplex DNA structures, taken both from human telomeres and from the proto-oncogene *c-myc*.

In the first part of the study, we tested the isoxazolo naphthoquinones **1a**–**h** by G4-FID (G-Quadruplex Fluorescence Intercalator Displacement) experiments in order to evaluate the affinity for DNA fragments and the selectivity for G-quadruplex compared to duplex DNA structures. In a second step, the most promising compounds (**1a** and **1b**) were tested by NMR experiments in the presence of model oligonucleotides of both G-quadruplex and double-stranded DNA . The G-quadruplex-forming DNA sequences and the control DNA duplexes are shown in Table 1.

2. Materials and methods

2.1. Sample preparation

The oligonucleotides were synthesized in 1 μmol scale on an Applied Biosystems DNA/RNA 3400 synthesizer by solid-phase 2-cyanoethylphosphoroamidite chemistry. They were passed through a cation exchange resins, Dowex 50WX2 and then desalted in a Sephadex (NAP-10) G25 column. The NMR samples of $d(T_2G_3T_2)_2$, $d(TAG_3T_2A)_4$ and $d(T_2AG_3T)_4$ were prepared at a 0.25–0.40 mM in G-quadruplex concentration range, in H_2O/D_2O (9:1) containing 25 mM KH_2PO_4, 150 mM KCl and 1 mM EDTA (pH 6.7). The NMR samples of Pu22 were prepared at 0.34 mM concentration in G-quadruplex in H_2O/D_2O (9:1) in the absence and in the presence of 25 mM KH_2PO_4, 70 mM KCl (pH 6.9). The oligonucleotides were heated to 85 °C for 1 min and then cooled at room temperature overnight.

Table 1
Oligonucleotide sequences used in this study.

DNA code	5′-sequence-3′
ds26	CAA TCGGAT CGA ATT CGA TCC GAT TG
c-myc	TGG TGA GGG TGG G**G**A GGG TGG G**G**A AGG TGG GG
Pu22	TGA GGG TGG G**T**A GGG TGG G**T**A A
24bcl	CGG GCG CGG GAGGAA GGG GGC GGG
HT24	TAG GGT TAG GGT TAG GGT TAGGGT
T_2AG_3T	TTA GGG T
TAG_3T_2A	TAG GGT TA
$T_2G_3T_2$	TTG GGT T
ds8	CGT ATA CG

A stock solution of drugs was prepared in DMSO-d6 at the concentration of 20 mM.

2.2. G-quadruplex fluorescence intercalator displacement experiments (G4-FID)

A 0.5 μM thiazole orange (TO) solution was mixed with 0.25 μM solution of pre-folded oligonucleotide target in the presence of a 10 mM sodium cacodylate buffer with 100 mM KCl, pH 7.5 at 25 °C. Each ligand addition step (from 0.1 to 20 equivalents) has been followed by a 10-min equilibration period after which the fluorescence spectrum is recorded from 510 to 650 nm (λ_{ex} = 501 nm). The percentage of displacement was calculated from the fluorescence height (FH, at 635 nm), using: percentage of displacement = 100 − [(FH/FH_0) × 100], where FH_0 is the fluorescence of TO bound to the oligonucleotide without ligand. The percentage of displacement was then plotted as a function of the concentration of added ligand.

The selectivity for the structures G-quadruplex vs. duplex was calculated on the basis of the percentage of displacement of TO induced by a concentration equal to 10 μM of ligand in the presence of the double strand oligonucleotides (ds26). Therefore, the concentration of ligand required to obtain the same percentage of displacement of TO in the

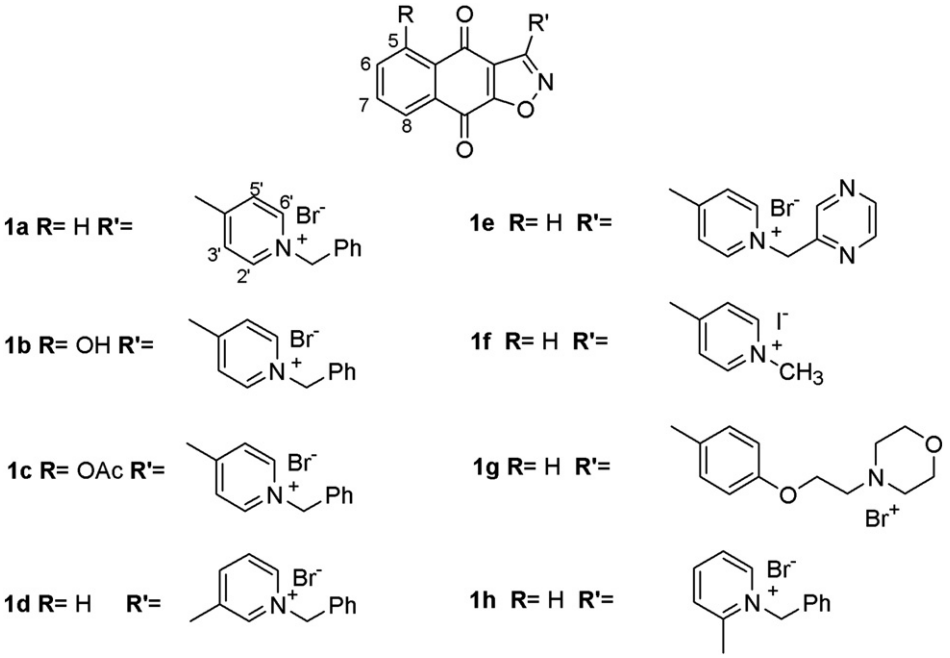

Fig. 1. Structure of naphthoquinone derivatives **1a**–**h**.

presence of a G-quadruplex (^{G4}C), allows for estimating the selectivity by the following equation:

$$\text{Estimated selectivity} : 10\mu M/{}^{G4}C\mu M$$

2.3. NMR experiments

The NMR spectra were recorded on a Bruker AV600 spectrometer operating at a frequency of 600.10 MHz for ^{1}H nucleus at variable temperature ranging from 5 °C to 85 °C. Chemical shifts (δ) were measured in ppm. ^{1}H NMR spectra were referenced to external DSS (2,2-dimethyl-2-silapentane-5-sulfonate sodium salt) set at 0.00 ppm.

^{1}H NMR titrations were performed by adding increasing amounts of the drug to the oligonucleotide solution until R = [ligand]/[DNA] = 4.0 was reached and in inverse order, by adding increasing amounts of DNA to a solution of drug from R = 60 to R = 15.

^{1}H assignments for the drugs in free and bound species were performed by using NOESY, ROESY and TOCSY experiments. Phase sensitive NOESY spectra were acquired at different R ratio at 25 °C and 40 °C in TPPI mode, with 2048 × 1024 complex FIDs. Mixing times ranged from 100 ms to 500 ms. TOCSY spectra were acquired with the use of a MLEV-17 [31] spin-lock pulse (60 ms total duration). All spectra were transformed and weighted with a 90° shifted sine-bell squared function to 4 K × 4 K real data points. The program Sparky [32] was used to assign the NOESY cross-peaks. The G-quadruplex $d(TAG_3T_2A)_4$ [33], $d(T_2AG_3T)_4$ [34] and $d(T_2G_3T_2)_4$ [35,36] were previously assigned.

2.4. Molecular modeling experiments

The studied derivatives (**1a** and **1b**) were refined using a systematic conformer search followed by geometry optimization of the lowest energy structure with MOPAC7 (PM3 Method, RMS gradient 0.0100).

The $d(T_2AG_3T)_4$ model was obtained following the directions previously described [37]. In order to obtain the $d(T_2G_3T_2)_4$ model, the coordinates from the solution NMR structures of G-quadruplex DNA telomeric repeat $d(T_2G_4T)_4$ (Protein Data Bank entry 139D) were taken as a starting structure. The G-tetrad was mutated to T4 and the model was subjected to molecular mechanics energy minimization (5000 steps steepest descent and 3 × 1000 steps conjugate gradient), followed by 500 ps of molecular dynamics simulation (1.0 fs time step at 298 K). The subsequent time-averaged structure was further minimized (1000 steps steepest descent and 3 × 1000 steps conjugate gradient) and used as the basis for all further modeling studies.

The ligand binding site was introduced in the G5pT6 step by breaking two phosphate backbones and separating the two halves of the structure so that the separation of G5 from T6 increased to 7 Å. The sugar-phosphate chains were reconnected, and molecular mechanics energy minimization (1000 steps steepest descent followed by 1000 steps conjugate gradient) was used to relieve any resulting steric distortion, while retaining the intercalation geometry between the GpT quartets by means of appropriate positional restraints. Energy minimizations and MD calculations were performed using the GROMACS package [38] using the GROMOS 53a6 force field [39].

Molecular docking experiments were performed with Autodock 4.0 [40,41]. We used the Lamarckian Genetic Algorithm which combines global search (Genetic Algorithm alone) to local search (Solis and Wets algorithm) [42]. **1a** and **1b** and the G-quadruplexes were further processed using the Autodock Tool Kit (ADT) [43]. Gasteiger–Marsili charges [44] were loaded on the ligands in ADT and Cornell parameters were used for the phosphorous atoms in the DNA. Solvation parameters were added to the final structure using Addsol utility of Autodock. Each docking consisted of an initial population of 50 randomly placed individuals, a maximum number of 200 energy evaluations, a mutation rate of 0.02, a crossover rate of 0.80, and an elitism value of 1. For the local search, the so-called pseudo-Solis and Wets algorithm was applied using a maximum of 250 iterations per local search. 250 independent docking runs were carried out for each ligand. The grid maps representing the system in the actual docking process were calculated with Autogrid. The dimensions of the grids were 80 × 80 × 50, with a spacing of 0.2 Å between the grid points and the center close to the cavity left by the ligand after its removal. The simpler intermolecular energy function based on the Weiner force field in Autodock was used to score the docking results. Results differing by less than 1.0 Å in positional root-mean-square deviation (rmsd) were clustered together and represented by the result with the most favorable free energy of binding. We also classified the resulting binding mode by visual inspection.

3. Results and discussion

3.1. Fluorescence experiments

The thiazole orange dye (TO) fluorophore is known to bind (K_a = 2×10^6 M^{-1}) both G-quadruplex and duplex DNA structures with high affinity [45]. With these experiments, it is possible to observe the displacement of the TO fluorophore by our ligands and evaluate their efficiency in doing it. The values of DC_{50} reported in Table 2 for compounds **1a**–**h** gave a preliminary indication of a high selectivity toward the G-quadruplex structures. Most of the naphthoquinone derivatives can be considered as moderate TO-displacer for 24bcl and HT24, whereas some of them reveal a strong affinity for the promoter sequence of the proto-oncogene *c-myc*. Compounds **1a**–**c** and **1e**–**f** (Fig. 1), with the positively charged pyridine nitrogen in para position relatively to the isoxazolo naphthoquinone, showed a high affinity for *c-myc* G-quadruplex, in particular when the nitrogen is bound to a benzyl substituent. In the case of compounds **1 h** and **1d**, the presence of the charged nitrogen atom of pyridine ring in meta and ortho with respect to the isoxazolo naphthoquinone moiety does not allow a significant interaction with the negative surface of the oligonucleotide. This is attributed to a conformational rigidity and an increased steric effect of the molecule. Bhattacharya and coworkers reported a similar effect of pyridine based ligands on DNA binding [46]. Finally, **1g** showed a good affinity for c-*myc* sequence, while a poor affinity was observed toward the other sequences used. Interestingly, all the compounds failed to displace TO in the presence of ds26 duplex structure, whereas they indicate a selected affinity to G-quadruplex DNA structures.

3.2. Mode of binding of selected compounds with G-quadruplex by NMR spectroscopy

On the basis of the results obtained by fluorescence assays, compounds **1a** and **1b** were selected to study the interaction with model oligonucleotides by NMR. We firstly performed NMR experiments with a double helix DNA to confirm the G-quadruplex over duplex selectivity of isoxazolo naphthoquinone compounds, as indicated by G4-FID

Table 2
DC_{50} (μM) of compounds **1a**–**h**[a].

Ligand	DC_{50} (μM)			
	ds26	24bcl	HT24	c-myc
1a	>10	3.5	4.0	1.1
1b	>10	2.5	3.5	0.8
1c	>10	2.5	3.0	0.4
1d	>10	6.0	2.1	2.1
1e	>10	9.0	>10	2.0
1f	>10	8.0	4.5	1.3
1 g	>10	>10	>10	3.5
1 h	>10	>10	>10	>10

[a] DC_{50} stands for the concentration required for 50% displacement of TO into G-quadruplex and duplex DNA (experimental errors estimated at ±5%). The classical TO-displacers are considered moderate or strong when the values of DC_{50} are between 1 and 2.5 μM, or between 0.1 and 1 μM, respectively [45].

results. The titration experiment conducted with the self-complementary oligonucleotide d(CGTATACG)$_2$ showed that **1a** does not interact with duplex oligonucleotide, as no chemical shift or line broadening variations occur (data not shown).

Different oligonucleotides were used as models of DNA G-quadruplex structures: d(T$_2$AG$_3$T)$_4$, d(TAG$_3$T$_2$A)$_4$, d(T$_2$G$_3$T$_2$)$_4$. The first sequence contains the entire fundamental unit of human telomere (TTAGGG)$_n$ and presents a further thymine at the 3′-end, which prevents the formation of aggregates, known to occur [47], due to the "end-to-end" stacking interactions between G-tetrads of different oligomers. We have then considered for our study the known oligonucleotide Pu22 [48], which contains two G to T mutations at 14 and 23 positions with respect to the *c-myc* sequence present in a gene promoter region (Table 1).

3.2.1. ^{1}H NMR experiments and molecular modeling on the [**1a**]/[d(T$_2$AG$_3$T)$_4$] complex

The titration experiments showed a significant up-field variation for the protons of the naphthoquinone residue and for the NH imino resonances, particularly concerning the external tetrads (Tables 3 and 1S). At a ratio R = 2, the chemical shift of the imino protons appears almost unchanged, suggesting a saturation of the binding sites and a stoichiometry of two molecules of ligand per G-quadruplex (Fig. 2). Melting experiments confirmed the stabilization of the G-quadruplex structure by **1a**: T_m of the complex (≈80 °C) is increased by ≥15 °C compared to T_m of the oligonucleotide alone (Fig. 1S).

The ligand leads to a slight line broadening of the NHG4 signal (Fig. 2), which is interpreted as a certain mobility of **1a** within the binding site. This is confirmed by a considerable line broadening of the protons of the ligand, in particular those of the naphthoquinone residue, reflecting changes in the local environment.

The NOESY spectra indicated that the binding occurs at two sites, i.e. at the level of ApG and GpT steps. The naphthoquinone protons show NOE contacts with NHG4, while the pyridine protons show correlations with A3, G4 and G6 (Fig. 3). The phenyl moiety, in addition to the NOE contacts with G4, also interacts with T2, G5 and G6 residues (Table 4). The fundamental NOEs, attesting the presence of the A-tetrad in the free d(T$_2$AG$_3$T)$_4$ G-quadruplex, involve the NH2 group of A3 with NHG4 and H2A3 [34,49]. The NH2A3 signal has been identified in our complex at 6.88 ppm, but it does not show NOE with the aromatic H2 resonance, which excludes the maintenance of the hydrogen bonds of the A-tetrad. In addition, the amino proton resonance of the adenines experiment an up-fields shift (0.23 ppm), that can be interpreted as both the break of the hydrogen bonds and the effect of the ring current induced by the ligand, stacked at the A3pG4 step. The important NOE interactions involving the G4 unit prove the intercalation of **1a** between A3 and G4, which consequently induces a distortion of the A tetrad plane. The fact that the phenyl moiety presents at the same time NOE contacts with T2 and G5 units suggests that the benzyl ring has a conformational mobility and can therefore assume different orientations within the binding site A3pG4.

The interaction of the ligand at the second site, G6pT7, follows from the NOE contacts of the pyridine and phenyl moieties with NHG6 and H5′G6, together with the significant up-field shift of NHG6. The ligand must be stacked over the G6-tetrad, which consequently pushes away the T7 unit, thus missing the π-interactions with the guanines, as shown by the low-field shift of H6 and Me protons of T7.

The geometry of the complex between **1a** and d(T$_2$AG$_3$T)$_4$ has been characterized by docking experiments performed on the basis of the experimental NOEs. The positions of the naphthoquinone core, external and orthogonal to the G-tetrads, were discarded because in contrast with the experimental data. The analysis of the remaining structures

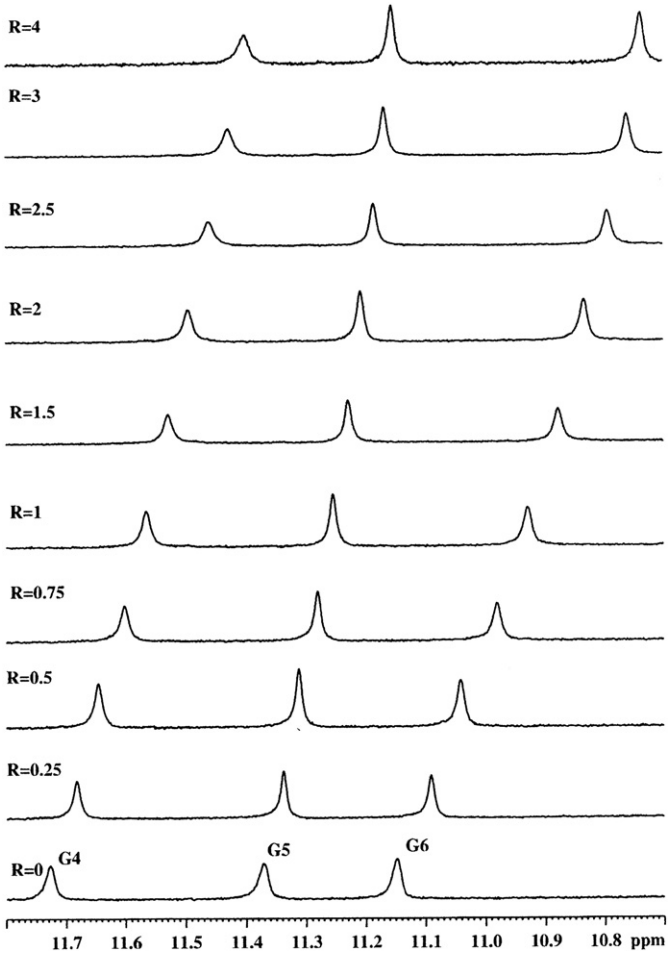

Fig. 2. ^{1}H NMR spectra (11.8–10.7 ppm) of the complex [**1a**]/[d(T$_2$AG$_3$T)$_4$], acquired at T = 40 °C in H$_2$O, containing 25 mM KH$_2$PO$_4$, 150 mM KCl and 1 mM EDTA (pH 6.7), showing the resonance of the imino protons of G4, G5 and G6 at different R values.

Table 3
Selected ^{1}H chemical shift values of d(T$_2$AG$_3$T)$_4$ and d(T$_2$G$_3$T$_2$)$_4$ in the presence of **1a** and **1b**.[a]

[d(T$_2$AG$_3$T)$_4$]/[1a]	NH/NH$_2$	Δδ[b]	H8/H6	Δδ	H2/CH$_3$	Δδ
T1	–	–	7.55	0.04	1.79	−0.01
T2	–	–	7.49	0.07	1.90	0.00
A3	6.88	**−0.23**	8.47	−0.04	8.08	**−0.12**
G4	11.41	**−0.31**	8.00	−0.04	–	–
G5	11.16	**−0.21**	7.76	−0.10	–	–
G6	10.74	**−0.40**	7.86	0.05	–	–
T7	–	–	7.70	**0.22**	1.94	**0.18**
[d(T$_2$G$_3$T$_2$)$_4$]/[1a]	NH	Δδ	H8/H6	Δδ	CH$_3$	Δδ
T1	–	–	7.56	−0.13	1.62	−0.11
T2	–	–	7.55	−0.01	1.58	0.00
G3	11.23	**−0.41**	8.09	−0.14	–	–
G4	11.04	**−0.27**	7.71	−0.17	–	–
G5	10.44	**−0.51**	7.77	0.07	–	–
T6			7.62	**0.31**	1.89	**0.21**
T7	–	–	7.46	0.04	1.44	−0.01
[d(T$_2$G$_3$T$_2$)$_4$]/[1b]	NH	Δδ	H8/H6	Δδ	CH$_3$	Δδ
T1	–	–	7.68	−0.01	1.69	−0.04
A2	–	–	7.56	0.00	1.53	−0.05
G3	11.46	**−0.18**	8.17	−0.06	–	–
G4	11.14	**−0.17**	7.80	−0.08	–	–
G5	10.58	**−0.37**	7.79	0.09	–	–
T6	–	–	7.60	**0.29**	1.86	**0.18**
T7	–	–	7.48	0.06	1.66	0.01

The most representative chemical shift variations are reported in bold.
[a] The complex with d(T$_2$AG$_3$T)$_4$ was measured at 40 °C, those with d(T$_2$G$_3$T$_2$)$_4$ at 25 °C, in ppm (δ). Solution: H$_2$O containing 25 mM KH$_2$PO$_4$, 150 mM KCl, 1 m M EDTA, pH = 6.7. R = 4.
[b] (Δδ = δ$_{bound}$ − δ$_{free}$).

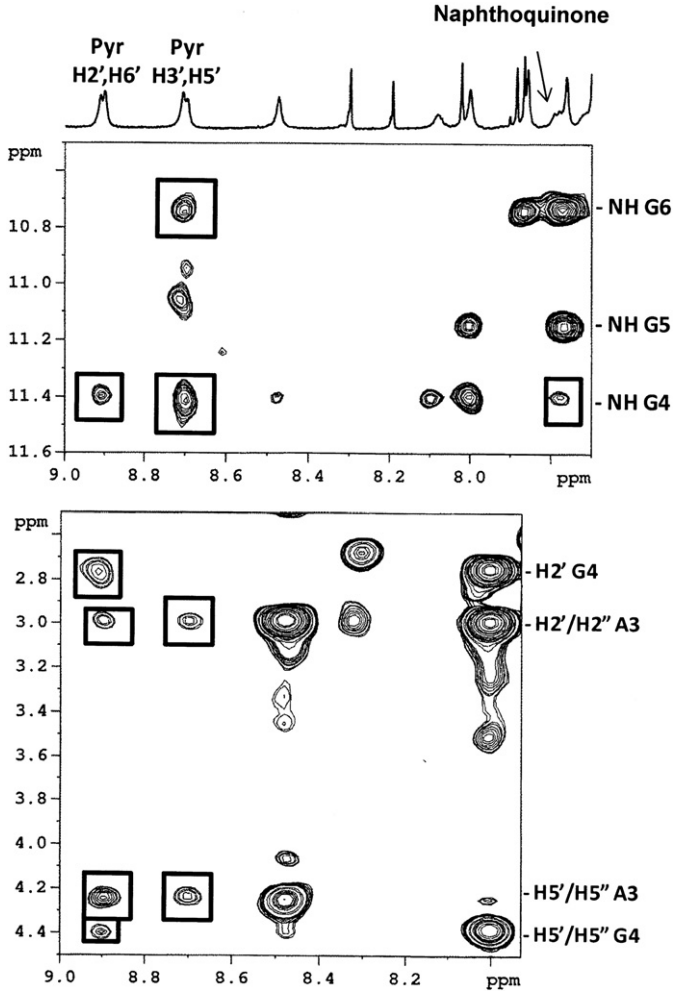

Fig. 3. Selected region of 2D NOESY spectrum of [**1a**]/[d(T_2AG_3T)$_4$] complex in the same conditions reported in Fig. 2). The boxes show the intermolecular NOEs between pyridine and naphthoquinone protons with different protons of d(T_2AG_3T)$_4$, highlighting two binding sites.

Table 4
Intermolecular NOE contacts of **1a** and interatomic distances (Å) with d(T_2AG_3T)$_4$ [a].

Binding site 1 (A3pG4)			
NOEs		Distance (Å)	
1a	d(T_2AG_3T)$_4$	Orientation 1[b]	Orientation 2[b]
H3′, H5′ pyridine	H8 A3	3.96	3.56
H3′, H5′ pyridine	H1′A3	4.97	4.73
H3′, H5′ pyridine	H2′, H2″ A3	2.75, 2.75	2.99, 4.06
H3′, H5′ pyridine	NH G4	4.67	3.88
H2′, H6′ pyridine	H8 A3	4.70	2.60
H2′, H6′ pyridine	H2′, H2″ A3	3.72, 4.61	2.83, 3.99
H2′, H6′ pyridine	H2′ G4	–	4.08
H2′, H6′ pyridine	H5′, H5″ G4	–	3.60, 5.17
Phenyl	H4′ T2	2.71	–
Phenyl	H4′ G4	2.38	–
Phenyl	H5′, H5″ G4	4.73, 5.31	3.62, 4.68
Phenyl	H4′ G5	–	3.80
Naphthoquinone	NH G4	3.20	2.99
Binding site 2 (G6pT7)			
H3′, H5′ pyridine	NH G6	3.08	
H2′, H6′ pyridine	H5′G6	4.86	
Phenyl	H5′ G6	4.01	

[a] See footnote (a) of Table 3.
[b] Docking energy −7.4 kcal/mol for orientation 1 and −6.1 kcal/mol for orientation 2.

confirms that **1a** behaves as a true intercalating agent, with 96% of the docking poses showing the naphthoquinone core fitted completely within the G-quadruplex. **1a** is placed in the ApG pocket formed by the A3 and G4 bases belonging to the four strands. The ligand adopts a quasi centro-symmetric position. This gives simultaneous π–π stacking interactions between the aromatic ring of the ligand and the rings of adenine and guanine units. As shown in Fig. 4A and B, the side chain can be arranged in two different ways, giving rise to two possible orientations, 1 and 2, which represent the 72% and 28% of the total population, respectively. In both cases the pyridine faces the negatively charged phosphodiester skeleton, but the positively charged nitrogen is closer to the phosphate in orientation 1 (3.53 Å) than in orientation 2 (4.77 Å). The benzyl group follows the trend of the grooves between the strands, toward G4 in orientation 1 and toward A3 in orientation 2 (Fig. 4A,B). Consequently the ligand must protrude at least partially from the binding site, thus allowing the rotation of the phenyl group. However, given the broadening of the NMR signals observed for both the oligonucleotide and the ligand, the interaction at the A3pG4 site could be better represented by an equilibrium between the two orientations. This hypothesis is also supported by the low difference observed for the binding energies between the two orientations.

The interaction of **1a** at the second site, G6pT7, was also examined by docking studies, which allowed visualization of the stacking of the ligand on the G-tetrad and the opening of the terminal thymine residues (Fig. 4C).

In order to better explore this site, G6pT7, we have examined the interaction with the G-quadruplex d(TAG_3T_2A)$_4$, which contains an external A residue more, over the thymines units. The experiments showed that **1a** forms a 2:1 complex, but the additional adenine units do not induce a major stabilization with respect to the above complex. The ligand is bound at ApG and GpT steps as results from the NOE interactions (data not reported).

*3.2.2. Interaction of **1a** and **1b** with d($T_2G_3T_2$)$_4$. ^{1}H NMR experiments and molecular modeling*

Another sequence related to human telomerase, d($T_2G_3T_2$)$_4$, was considered for the binding studies, in order to see the role of the adenine moieties over the G-tetrad in the interaction with the ligand. The titration with **1a** allowed for deriving the stoichiometry of two molecules of ligand per G-quadruplex. The NH imino protons of G3 and G5 (Table 3 and Fig. 2S) move up-field ($\Delta\delta = -0.4/-0.5$ ppm) while the aromatic and methyl protons of T6 move low-field ($\Delta\delta = +0.2/+0.3$ ppm). The intermolecular NOEs (Table 2S and Fig. 3S), involving the pyridine protons and G5 and T6 units, indicate that the pyridine is well superimposed on the G-tetrad. The phenyl is located close to the backbone of the strands, facing to the 5′-direction, as suggested by the NOE contacts with the ribose protons of G5. Another set of intermolecular NOEs, involving the ligand and the bases T2 and G3, indicates a second site of interaction at the level of T2pG3. The location of the ligand in the two sites, T2pG3 and G5pT6, is confirmed by the modeling (see below). Melting experiments indicate that the interaction of **1a** provides a good stabilization of the G-quadruplex structure ($\Delta T_m \leq 15$ °C), but it seems lower with respect to the complex with d(T_2AG_3T)$_4$ (Fig. 4S). In addition, a new set of three guanine NH imino protons appears down-field, indicating that a different mode of binding, rather than the end stacking, can occur (Fig. 2S). The intensity of the new signals was too low to be used for NOE experiments. Actually the thymine units are more flexible than the adenines and usually do not form a tetrad. Consequently, after a first step of stacking, the ligand can go out of the G-quadruplex and bind in a different mode or in a different binding site. This result confirms that the adenine moieties in d(T_2AG_3T)$_4$ stabilize the G-quadruplex structure in the complex.

Analogue **1b** presents a hydroxyl group on the naphthoquinone moiety, which may be involved in hydrogen bonding with the oligonucleotide, thus leading to a possible major stabilization of the complex with respect to **1a**. The titration experiments showed the same line

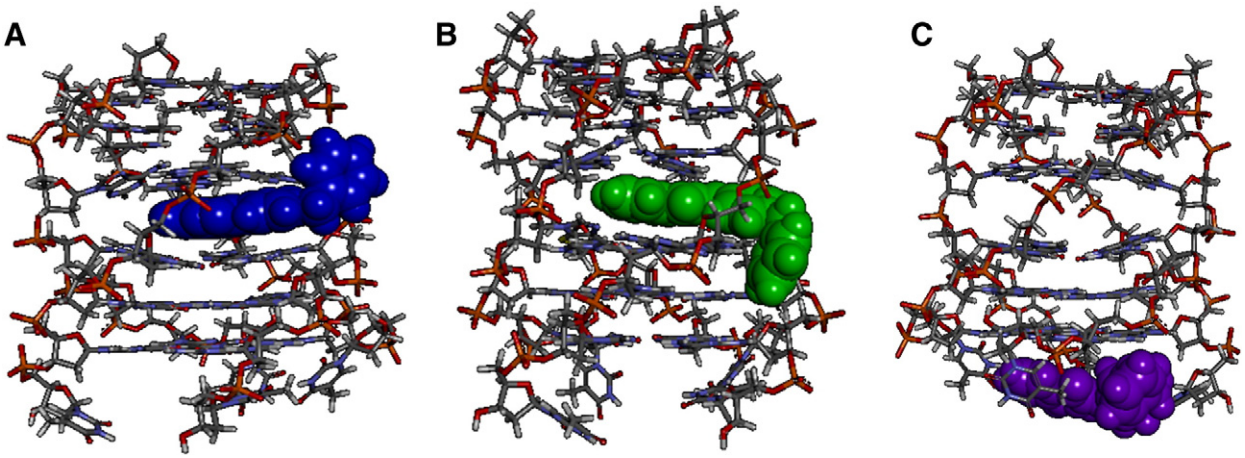

Fig. 4. Side views of the best docked conformations for **1a** in the two binding sites of the complex with $d(T_2AG_3T)_4$: **1a** in A3pG4 in orientation 1 (A) and 2 (B) and in G6pT7 step (C).

broadening observed for **1a**, but the set of new NH signals is absent (Fig. 5S). This could suggest a major stabilization, but the melting experiments gave a similar ΔT_m. A large number of NOE contacts involve several protons of G5, T6 and T7 with pyridine and naphthoquinone moieties (Table 2S), indicating that the G5pT6 step is the primary site of interaction also for **1b**. A smaller number of NOEs involve the T2pG3 step, showing that this ligand is also inserted in this position.

The comparison between the models of the two complexes allowed detection of small differences in the mode of binding. In the docking poses, the planar naphthoquinone moiety of both complexes fitted completely in the GpT binding pocket, formed by the G5 and T6 units of the four strands. In this case, the two ligands do not adopt the quasi centro-symmetric stacking interaction observed in the complex [**1a**]/[$d(T_2AG_3T)_4$], but are offset, with the center of the G-quadruplex occupied only by the aromatic moiety of the naphthoquinone (Fig. 6S). However the π–π stacking interactions between the ligands and the adjacent G-tetrad are still possible. The pyridine ring is always located in proximity of the negative phosphodiester groups. The benzyl group lies in the groove between the filaments and is directed toward T6, forming favorable hydrophobic interactions with the sides of the groove. The distances between the positively charged nitrogen of the pyridine and the nearest phosphate group are 3 Å and 2.72 Å for the complex with **1a** and **1b** respectively. These positions of **1a** and **1b** are both able to satisfy the experimental NOEs. The presence of alternative conformations of the benzyl group, as observed for the complex with $d(T_2AG_3T)_4$, was found here to be much less likely, with a percentage relative to the total population of ≈5%. In the case of **1b** compared with **1a**, the complex appears stabilized by a strong hydrogen bond (2.36 Å) between the phenolic OH and 3NH of T6. This can explain the absence of NH imino signals, due to other conformations, because the hydrogen bond fixes the ligand **1b** inside the complex.

3.2.3. Induction of G-quadruplex formation for c-myc Pu22 sequence by ***1a***

Pu22 is a 22 bases sequence of *c-myc*, with two mutations from G to T in positions 14 and 23 with respect to the native sequence (Table 1). These mutations restrict the number of isomers that may be in dynamic equilibrium in solution, and therefore allow the formation of a single parallel G-quadruplex structure [50]. The ^{1}H NMR spectrum of Pu22 at 25 °C has been interpreted by following the complete assignment in the literature [48].

The interaction of **1a** with Pu22 (Fig. 5) induces a dramatic change of the spectrum. At low R values (0.5–1.0) we observed the broadening of almost all the NH signals. These signals became sharp at R = 2, suggesting the formation of a well defined complex. All the 12 imino protons of the guanines are well resolved, which indicates that the core of the G-quadruplex is maintained. Then the spectrum does not significantly change for R = 2–4, which allows for determining the stoichiometry of 2 ligands *per* G-quadruplex.

NOESY experiments (Fig. 7S) of the complex led to the assignment of all the NH imino resonances of the guanines. The starting point was the up-field signal of NHG9 at 10.39 ppm which undergoes only a slight shift variation. NHG8 and NHG7 were consequently assigned by sequential NOEs. In the same way NHG16, G17 and G18 were assigned, starting from the down-field peak of NHG16. The NH of G20 is easily followed in the spectra and allows the assignment of also NHG21 and NHG22. The remaining signal at the upper field must be NHG13, as the other signals in this region have already been attributed. This leads to the assignment of NHG11 and NHG12 resonances. All the

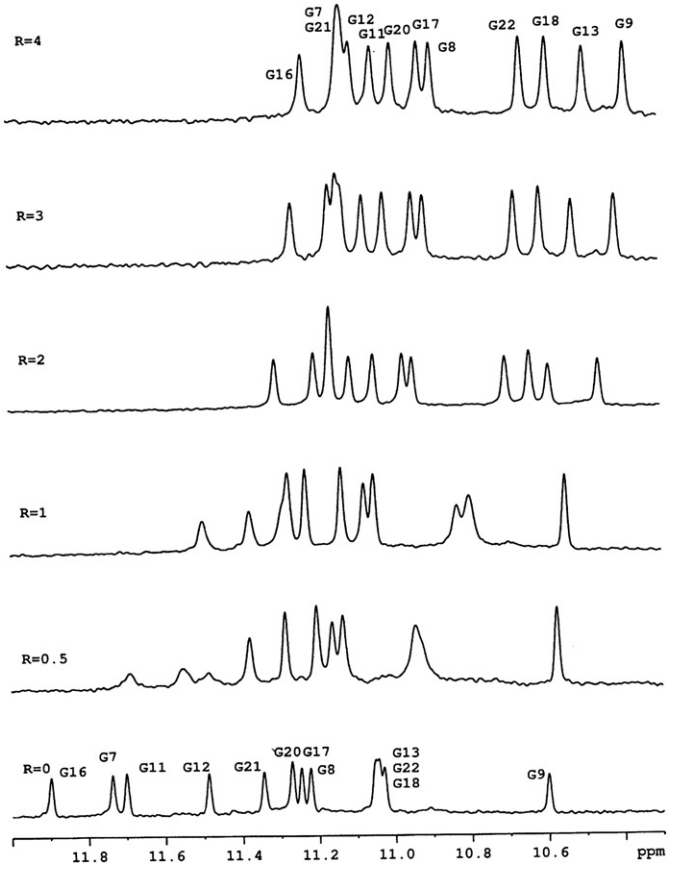

Fig. 5. ^{1}H NMR spectra (12.0–10.3 ppm) at different R = [**1a**]/[Pu22], at T = 25 °C in H_2O, with 25 mM KH_2PO_4, 70 mM KCl (pH 6.9), showing the resonances of the imino protons.

imino protons experience an up-field shift, which in the case of the most broad signals, i.e. NHG7, NHG11 and NHG16, is greater than 0.6 ppm, suggesting that there is an interaction between the ligand and the oligonucleotide, involving the tetrad G7–G11–G16–G20 (Table 3S). The intermolecular NOEs (Table 4S) involving NHG16 and NHG7 with the pyridine moiety of **1a** confirm the binding site. Other NOE interactions between phenyl and pyridine moieties with the NH imino protons of G9, G13, G22, allowed identification of the second binding site. The aromatic protons, H8 of A6, H2 of A24 and H8 of A25, suffer a considerable line broadening (Fig. 8S). This confirms that a ligand molecule is located over the tetrad G7–G11–G16–G20, and that a second ligand molecule is located over the tetrad G9–G13–G18–G22.

To better visualize the arrangement of ligand molecules within the G-quadruplex structure of Pu22, a preliminary model was constructed. The ligand has been forced to occupy the positions starting with our NMR data. Fig. 9S shows that the planar moiety of the ligand is parallel to the plane of the G-tetrads, affecting the conformations of the adenines and thymine T23, which represent the flexible extremes of the strand.

Although most of the research is focused on the ability of a ligand to stabilize the G-quadruplex structure, the importance of ligands that can induce the formation of G-quadruplex in the absence of cations cannot be neglected. For this reason, NMR titration experiment by adding **1a** to a solution of Pu22 in the absence of potassium or sodium has been performed, in order to detect the structural changes caused by the ligand. As shown in Fig. 6, the oligonucleotide is single-stranded in the absence of salts and signals related to the imino protons of the guanines in the down-field region (between 10 and 12 ppm) are not present. The addition of **1a** leads to the appearance of the guanine NH resonances, remarkably showing that the ligand has the ability to induce the formation of a G-quadruplex structure from a single strand. Comparing the spectra of the complexes obtained in the presence and in the absence of salts no common imino resonances can be recognized, suggesting that **1a** does not generate the formation of a unique G-quadruplex structure, but induces a dynamic equilibrium of different conformations.

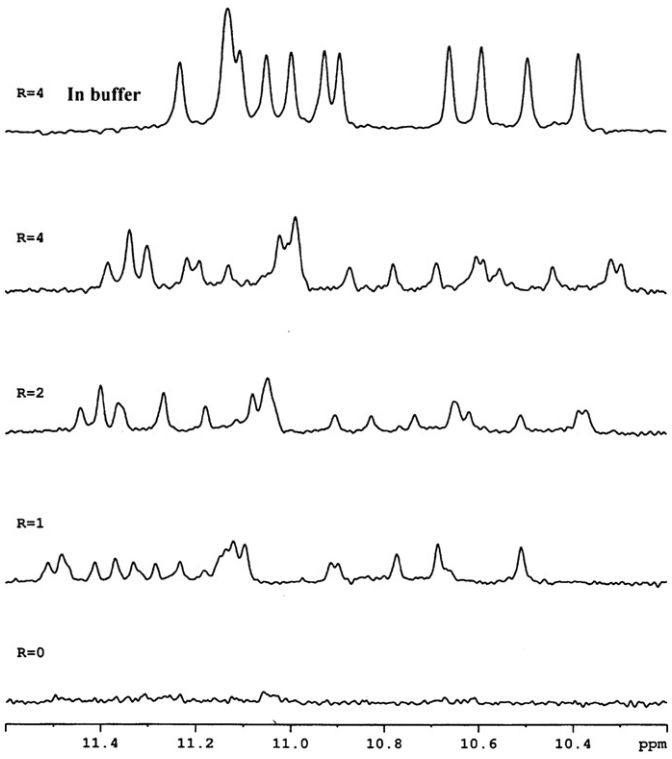

Fig. 6. Imino proton region of Pu22 in H_2O in the absence of salts (R = 0) and with the addition of **1a** with increasing R values. At the top the same region at R = 4.0 in the presence of salts.

4. Conclusion

A series of isoxazolo naphthoquinone derivatives, **1a**–**h**, recently synthesized [26] have shown a strong antiproliferative activity on different human tumor cell lines. Fluorescence and NMR experiments have shown the preferred affinity for G-quadruplex DNA, compared to duplex DNA structures and allowed the selection of compounds **1a** and **1b**, for their significant affinity toward G-quadruplexes of great biological relevance.

In the presence of parallel G-quadruplexes $d(T_2AG_3T)_4$, $d(T_2G_3T_2)_4$ and $d(TAG_3T_2A)_4$, models of telomeric sequences, compound **1a** showed good ability of stacking interactions, with the formation of complexes with 2:1 stoichiometry. The external G-tetrads are directly involved in the interaction with the ligand, without alterations in the structure of the G-quadruplex core.

In the complex with $d(T_2AG_3T)_4$, **1a** is placed in the A3pG4 pocket formed by the A3 and G4 bases. The ligand is anchored in the binding site, both by π-stacking interaction between the naphthoquinone moiety and the DNA bases, and by electrostatic interaction between the positively charged pyridine and the negatively charged phosphate backbone of the G-quadruplex. In the second binding site, G6pT7, the ligand is stacked over the G6 tetrad, pushing away the terminal thymine residues. In the complex with $d(T_2G_3T_2)_4$, **1a** does not seem to be able to adopt the quasi centro-symmetric stacking interaction, observed for the former complex. In addition, a new set of NH signals at low fields indicates that the ligand can go out of the G-quadruplex and bind in a different mode or site. These results prove the role of the adenine moieties, which further stabilize the complex, as the A-tetrad can contribute to an enhanced stacking between the naphthoquinone moiety and the adenine residues.

Analogue **1b** binds to $d(T_2G_3T_2)_4$ with the same mode, but the hydroxyl group on the naphthoquinone moiety forms a strong hydrogen bond (2.36 Å) with 3NH of T6, thus leading to a relative stabilization of the complex, compared to **1a**. The absence of imino NH signals, due to other conformations, is an evidence of this.

Moreover **1a** showed very significant results with the sequence (Pu22) related to the promoter of oncogenes *c-myc*. Two molecules of ligand interact with the intramolecular G-quadruplex at the level of the more external G-tetrads, affecting the conformation of adjacent bases. This kind of binding not only stabilizes the G-quadruplex structure of Pu22, but also induces the G-quadruplex formation from a single strand.

All these findings underline the relevance of compounds **1a** and **1b** in the stabilization and formation of G-quadruplex, opening new perspectives for the rational drug design of new anticancer agents.

Acknowledgements

This work was partially supported by Grants from PRIN09 (2009Prot.2009J54YAP_005). Collaborative research was funded by an Italian–Spanish collaborative action (IT2009-0067).

Appendix A. Supplementary data

Supplementary data to this article can be found online at http://dx.doi.org/10.1016/j.bbagen.2014.12.002.

References

[1] J.L. Huppert, S. Balasubramanian, Prevalence of quadruplexes in the human genome, Nucleic Acids Res. 33 (2005) 2908–2916.
[2] S. Balasubramanian, S. Neidle, G-quadruplex nucleic acids as therapeutic targets, Curr. Opin. Chem. Biol. 13 (2009) 345–353.

[3] S. Chiarella, et al., Nucleophosmin mutations alter its nucleolar localization by impairing G-quadruplex binding at ribosomal DNA, Nucleic Acids Res. (2013), http://dx.doi.org/10.1093/nar/gkt001.
[4] S. Neidle, The structures of quadruplex nucleic acids and their drug complexes, Curr. Opin. Struct. Biol. 19 (2009) 239–250.
[5] J.L. Huppert, S. Balasubramanian, G-quadruplexes in promoters throughout the human genome, Nucleic Acids Res. 35 (2007) 406–413.
[6] S. Rankin, et al., Putative DNA quadruplex formation within the human c-kit oncogene, J. Am. Chem. Soc. 127 (2005) 10584–10589.
[7] L.M. Facchini, L.Z. Penn, The molecular role of Myc in growth and transformation: recent discoveries lead to new insights, FASEB J. 12 (1998) 633–651.
[8] S. Pelengaris, B. Rudolph, T. Littlewood, Action of Myc in vivo — proliferation and apoptosis, Curr. Opin. Genet. Dev. 10 (2000) 100–105.
[9] C.A. Spencer, M. Groudine, in: George F. Vande Woude, George Klein (Eds.), Advances in Cancer Research, vol. 56, Academic Press, 1991, pp. 1–48.
[10] K.B. Marcu, S.A. Bossone, A.J. Patel, myc function and regulation, Annu. Rev. Biochem. 61 (1992) 809–858.
[11] A. Siddiqui-Jain, C.L. Grand, D.J. Bearss, L.H. Hurley, Direct evidence for a G-quadruplex in a promoter region and its targeting with a small molecule to repress c-MYC transcription, Proc. Natl. Acad. Sci. 99 (2002) 11593–11598.
[12] C.L. Grand, et al., The cationic porphyrin TMPyP4 down-regulates c-MYC and human telomerase reverse transcriptase expression and inhibits tumor growth in vivo 1. This research was supported by grants from the NIH and the Arizona Disease Control Research Commission.1, Mol. Cancer Ther. 1 (2002) 565–573.
[13] C.L. Grand, et al., Mutations in the G-quadruplex silencer element and their relationship to c-MYC overexpression, NM23 repression, and therapeutic rescue, Proc. Natl. Acad. Sci. U. S. A. 101 (2004) 6140–6145.
[14] G. Biffi, D. Tannahill, J. McCafferty, S. Balasubramanian, Quantitative visualization of DNA G-quadruplex structures in human cells, Nat. Chem. 5 (2013) 182–186.
[15] S. Balasubramanian, L.H. Hurley, S. Neidle, Targeting G-quadruplexes in gene promoters: a novel anticancer strategy? Nat. Rev. Drug Discov. 10 (2011) 261–275.
[16] A. De Cian, et al., Targeting telomeres and telomerase, Biochimie 90 (2008) 131–155.
[17] J.D. Schonhoft, et al., Direct experimental evidence for quadruplex-quadruplex interaction within the human ILPR, Nucleic Acids Res. 37 (2009) 3310–3320.
[18] W. Zhou, N.J. Brand, L. Ying, G-quadruplexes—novel mediators of gene function, J. Cardiovasc. Transl. Res. 4 (2011) 256–270.
[19] N.W. Kim, et al., Specific association of human telomerase activity with immortal cells and cancer, Science 266 (1994) 2011–2015.
[20] W.C. Hahn, et al., Inhibition of telomerase limits the growth of human cancer cells, Nat. Med. 5 (1999) 1164–1170.
[21] A.M. Zahler, J.R. Williamson, T.R. Cech, D.M. Prescott, Inhibition of telomerase by G-quartet DMA structures, Nature 350 (1991) 718–720.
[22] D. Monchaud, M.-P. Teulade-Fichou, A hitchhiker's guide to G-quadruplex ligands, Org. Biomol. Chem. 6 (2008) 627.
[23] B. Maji, S. Bhattacharya, Advances in the molecular design of potential anticancer agents via targeting of human telomeric DNA, Chem. Commun. 50 (2014) 6422.
[24] S.M. Haider, S. Neidle, G.N. Parkinson, A structural analysis of G-quadruplex/ligand interactions, Biochimie 93 (2011) 1239–1251.
[25] A.K. Jain, S. Bhattacharya, Interaction of G-quadruplexes with nonintercalating duplex-DNA minor groove binding ligands, Bioconjug. Chem. 22 (2011) 2355–2368.
[26] A. Bargiotti, et al., Isoxazolo(aza)naphthoquinones: a new class of cytotoxic Hsp90 inhibitors, Eur. J. Med. Chem. 53 (2012) 64–75.
[27] J. Trepel, M. Mollapour, G. Giaccone, L. Neckers, Targeting the dynamic HSP90 complex in cancer, Nat. Rev. Cancer 10 (2010) 537–549.
[28] M. Bejugam, et al., Trisubstituted isoalloxazines as a new class of G-quadruplex binding ligands: small molecule regulation of c-kit oncogene expression, J. Am. Chem. Soc. 129 (2007) 12926–12927.
[29] M. Bejugam, et al., Targeting the c-Kit promoter G-quadruplexes with 6-substituted indenoisoquinolines, ACS Med. Chem. Lett. 1 (2010) 306–310.
[30] K.I.E. McLuckie, et al., G-quadruplex-binding benzo[a]phenoxazines down-regulate c-KIT expression in human gastric carcinoma cells, J. Am. Chem. Soc. 133 (2011) 2658–2663.
[31] A. Bax, D.G. Davis, MLEV-17-based two-dimensional homonuclear magnetization transfer spectroscopy, J. Magn. Reson. 1969 (65) (1985) 355–360.
[32] T.D. Goddard, D.G. Kneller, SPARKY 3, University of California, San Francisco, USA, 2004.
[33] M.J. Cocco, L.A. Hanakahi, M.D. Huber, N. Maizels, Specific interactions of distamycin with G-quadruplex DNA, Nucleic Acids Res. 31 (2003) 2944–2951.
[34] E. Gavathiotis, M.S. Searle, Structure of the parallel-stranded DNA quadruplex d(TTAGGGT)4 containing the human telomeric repeat: evidence for A-tetrad formation from NMR and molecular dynamics simulations, Org. Biomol. Chem. 1 (2003) 1650–1656.
[35] Q. Zhou, et al., Screening potential antitumor agents from natural plant extracts by G-quadruplex recognition and NMR methods, Angew. Chem. Int. Ed. 47 (2008) 5590–5592.
[36] Q. Shang, et al., Fishing potential antitumor agents from natural plant extracts pool by dialysis and G-quadruplex recognition, Talanta 85 (2011) 820–823.
[37] R. Ferreira, et al., Structure and stability of human telomeric G-quadruplex with preclinical 9-amino acridines, PLoS ONE 8 (2013) e57701.
[38] E. Lindahl, B. Hess, D. van der Spoel, GROMACS 3.0: a package for molecular simulation and trajectory analysis, Mol. Model. Annu. 7 (2001) 306–317.
[39] C. Oostenbrink, T.A. Soares, N.F.A. van der Vegt, W.F. van Gunsteren, Validation of the 53A6 GROMOS force field, Eur. Biophys. J. 34 (2005) 273–284.
[40] G.M. Morris, et al., Automated docking using a Lamarckian genetic algorithm and an empirical binding free energy function, J. Comput. Chem. 19 (1998) 1639–1662.
[41] R. Huey, G.M. Morris, A.J. Olson, D.S. Goodsell, A semiempirical free energy force field with charge-based desolvation, J. Comput. Chem. 28 (2007) 1145–1152.
[42] F.J. Solis, R.J.-B. Wets, Minimization by random search techniques, Math. Oper. Res. 6 (1981) 19–30.
[43] M.F. Sanner, Python: a programming language for software integration and development, J. Mol. Graph. Model. 17 (1999) 57–61.
[44] J. Gasteiger, M. Marsili, Iterative partial equalization of orbital electronegativity—a rapid access to atomic charges, Tetrahedron 36 (1980) 3219–3228.
[45] D. Monchaud, et al., Ligands playing musical chairs with G-quadruplex DNA: a rapid and simple displacement assay for identifying selective G-quadruplex binders, Biochimie 90 (2008) 1207–1223.
[46] P. Chaudhuri, B. Ganguly, S. Bhattacharya, An experimental and computational analysis on the differential role of the positional isomers of symmetric bis-2-(pyridyl)-1H-benzimidazoles as DNA binding agents, J. Org. Chem. 72 (2007) 1912–1923.
[47] Y. Kato, T. Ohyama, H. Mita, Y. Yamamoto, Dynamics and thermodynamics of dimerization of parallel G-quadruplexed DNA formed from d(TTAGn) (n = 3–5), J. Am. Chem. Soc. 127 (2005) 9980–9981.
[48] A. Ambrus, D. Chen, J. Dai, R.A. Jones, D. Yang, Solution structure of the biologically relevant g-quadruplex element in the human c-myc promoter. Implications for G-quadruplex stabilization†, Biochemistry (Mosc) 44 (2005) 2048–2058.
[49] Y. Wang, D.J. Patel, Guanine residues in d(T2AG3) and d(T2G4) form parallel-stranded potassium cation stabilized G-quadruplexes with anti glycosidic torsion angles in solution, Biochemistry (Mosc) 31 (1992) 8112–8119.
[50] J. Seenisamy, et al., The dynamic character of the G-quadruplex element in the c-myc promoter and modification by TMPyP4, J. Am. Chem. Soc. 126 (2004) 8702–8709.